http://dx.doi.org/10.21611/qirt.2012.233

Imaging detection of CO_2 using a bispectral type-II superlattice infrared camera

by F. Rutz*, R. Rehm*, A. Wörl*, J. Schmitz*, M. Wauro*, J. Niemasz*, M. Masur*, M. Walther*, R. Scheibner**, and J. Ziegler**

* Fraunhofer-Institut für Angewandte Festkörperphysik (IAF), Tullastr. 72, 79108 Freiburg, Germany
frank.rutz@iaf.fraunhofer.de
** AIM Infrarot-Module GmbH, Theresienstr. 2, 74072 Heilbronn, Germany

Abstract

Bispectral infrared (IR) cameras provide additional spectral information in contrast to common monospectral devices, which merely measure the integrated intensity of IR radiation. A bispectral IR camera has been manufactured from InAs/GaSb type-II superlattices. The two detector channels range from 3 – 4 µm and 4 – 5 µm, respectively. Thus, this camera is very sensitive to the spectral signature of carbon dioxide at approximately 4.3 µm and can be used for remote imaging of CO_2.

1. Introduction

Carbon dioxide, CO_2, is sometimes called the most important gas of the twenty-first century [1]. Because of its significant influence on the climate, imaging techniques that can monitor natural or industrial processes as sources for CO_2 emissions are gaining interest. Most molecular gases provide individual absorption / emission bands in the IR spectral range. These bands result from rotational-vibrational transitions and act as a »fingerprint« for the specific molecule. Usually, IR signatures of gases are selectively visualized utilizing narrow-band filters together with broad-band IR detection systems [1]. However, high-intense broad-band IR sources like, e.g., hot objects or solar reflections can be misinterpreted as IR emissions from hot gases since parts of the broad-band photon flux pass the narrow-band filter. In contrast, multispectral IR cameras differentiate between several bands in the IR range and can thus discern between various objects and gases due to their spectral signatures. Actually, a bispectral IR camera serves as an imaging spectrometer if one channel detects the absorption / emission band of a certain molecule and the other channel does not. In this paper, we will discuss how such a bispectral camera can be applied for qualitative and quantitative detection of CO_2.

2. Asymmetric stretching mode of CO_2

The infrared spectral range is divided into several »atmospheric windows«, corresponding to spectral bands that are (almost) unaffected by absorption lines of atmospheric gases. The black curve in Fig. 1 represents the atmospheric transmission as a function of wavelength. The bands from 3 µm to 5 µm and from 8 µm to 14 µm, called mid-wave infrared (MWIR) and long-wavelength infrared (LWIR), respectively, are very important since IR cameras and other IR systems operating in these band benefit from the long detection range. The spectral signature of the (00^01) asymmetric stretching mode of CO_2 lies isolated within the MWIR band and is relatively unaffected by contributions from other atmospheric gases [2]. However, the spectral mode comprises many rotational-vibrational transitions at slightly different energies. Moreover, the individual absorption coefficients are dependent on temperature, pressure, and gas composition. This complicates the simple usage of the Lambert-Beer law

$$I_\lambda = I_{0\lambda} e^{-\alpha_\lambda \rho l} \qquad (1)$$

with the measured intensity I_λ, the source intensity $I_{0\lambda}$, and the absorption coefficient α_λ at the wavelength λ, the gas density ρ, and the absorption path length l. Fourier-transform infrared (FTIR) spectrometers, Fabry-Pérot interferometers, or monochromators can resolve the individual spectral lines. Yet, the required measurement time restricts applications to slowly varying or static scenes, especially when imaging with high spatial resolution is desired. Such a high spectral resolution is not required for many applications. The full absorption band spanning several tens of nanometres wavelength is treated as a single spectral feature instead. Then, the Lambert-Beer law Eq. (1) is still a good approximation, if the variables remain in a limited range [2].

The measurements are usually affected by further attenuation effects, like absorption and scattering from dust particles in the air. This can be considered as an attenuation factor A in Eq. (1), which directly alters the calculation of the gas density ρ from Eq. (1). This can be suppressed by normalising the measurement of the absorption band $I_{,a}$ with a measurement of a reference band $I_{,r}$ in close spectral proximity:

$$I_a = A_a I_{0a} e^{-\alpha_a \rho l} \qquad (2)$$
$$I_r = A_r I_{0r} \qquad (3)$$

http://dx.doi.org/10.21611/qirt.2012.233

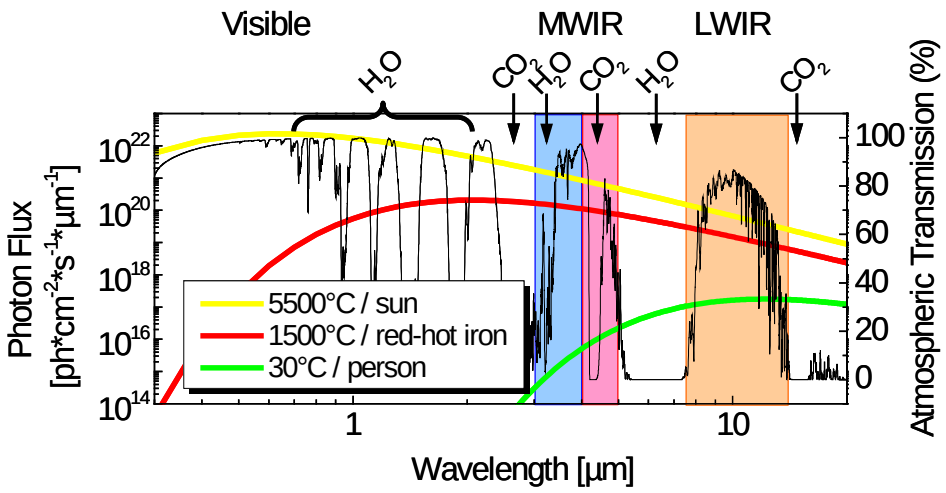

Fig. 1. *Photon flux density for various blackbody temperatures (yellow, red, and green curves) and atmospheric transmission (black curve) as functions of the photon wavelength.*

The attenuation factors can be considered as nearly equal, if the two bands are close to each other, i.e. $A_a = A_r = A$. The same holds for the source emissivity coefficients $\varepsilon_a = \varepsilon_r = \varepsilon$. Thus, with a constant source temperature, the source intensities

$$I_{0a} = \varepsilon I_{bb}(\lambda_a) \quad (4)$$
$$I_{0r} = \varepsilon I_{bb}(\lambda_r) \quad (5)$$

differ mostly due to the blackbody spectral radiance $I_{bb}(\lambda)$, which can be calculated from Planck's formula

$$I_{bb}(\lambda) = \frac{2\pi hc^2}{\lambda^5}\frac{1}{e^{ch/\lambda kT}-1} \quad (6)$$

for known values of the temperature T and the effective wavelength λ for each band, the Planck constant h, the speed of light c, and the Boltzmann constant k. From the ratio of Eqs. (2) and (3), the density of the absorbing gas can then be extracted via

$$\rho = -\frac{1}{\alpha_a l}\left[\ln\left(\frac{I_a}{I_r}\right) + \ln\left(\frac{I_{bb}(\lambda_r)}{I_{bb}(\lambda_a)}\right)\right]. \quad (7)$$

This only holds for optically thin volumes of absorbing gases. In many gas sensing applications, e.g. leak detection at industrial sites or remote emission control of smokestacks, IR radiation emitted from gases with higher temperatures occurs. In this case, the gas itself acts as a blackbody source according to Eq. (6) and the intensity *increases* with increasing path length. If the gas containing path length is long enough or the concentration is very high, the intensity saturates due to self-absorption. For such optically thick gas volumes, the measured emitted intensity I_e is [3]

$$I_e = I_{bb}(\lambda)(1 - e^{-\alpha_e \rho l}). \quad (2)$$

3. Bispectral type-II superlattice IR camera

In order to achieve an IR camera system that is capable of measuring the absorption band of the CO_2 asymmetric stretching mode as well as a reference band, the concept and photosensitive properties of such a bispectral detector have to be considered.

3.1. Bispectral detector concept

Several approaches exist to detect IR radiation in two (or more) spectral bands. First of all, with a broadband detector, covering both spectral bands, the shortwave and longwave IR radiation cannot be distinguished (see Fig. 2a). Using a dichroic mirror (Fig. 2b), the radiation from both bands can be separated and detected on individual (narrowband) detector arrays separately. This enables the simultaneous image acquisition of both bands. However, the optical alignment and exact superposition of both images is delicate and the whole system gets rather bulky. A broadband detector equipped with a matrix filter (Fig. 2c) analog to the »Bayer filter« (for red, green, and blue in the visible range, used by most digital cameras) allows for simultaneous bispectral IR detection, too, with the expense of a lower spatial resolution and a non-perfect pixel registration. Very common is a spinning filter wheel (Fig. 2d) in front of a broadband IR detector, facilitating a frame-by-frame sequence of alternating shortwave and longwave IR images. Obviously, no synchronous detection in both bands is possible this way. A bispectral IR detector in stacked configuration is illustrated in Fig. 2e. Its front detector array is sensitive for the shortwave radiation but, due to the specific photodetection properties, transparent for the longwave radiation, which is absorbed in the second detector array behind the first one. With this configuration, a simultaneous and pixel-registered measurement of both IR bands is guaranteed.

Using a bispectral (MWIR/LWIR dual-band) IR camera with stacked detectors, the absolute temperature of a grey body can be measured without the explicit knowledge of the emissivity of the object. The temperature of the object under observation is derived by the ratio of the emitted radiation in two spectral bands and fitted to an adequate Planck curve [4]. Furthermore, active thermography on infrared transparent materials [5] can also benefit from the synchronous and pixel-registered recording of transient thermal phenomena.

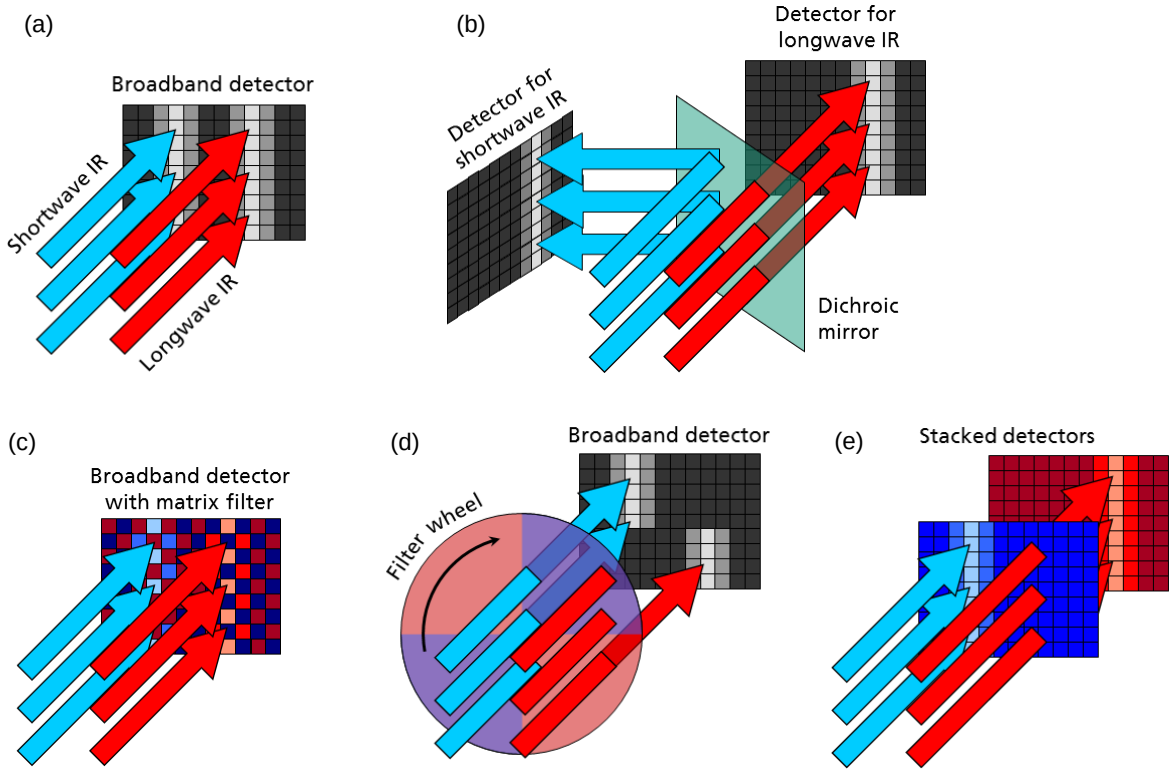

Fig. 2. *Different approaches for imaging infrared radiation in two spectral bands: Broadband detector (a), two detector arrays with dichroic mirror (b), broadband detector with filter matrix (c), broadband detector with filter wheel (d), and stacked detector arrays (e).*

3.2. InAs/GaSb type-II superlattices

For the realisation of a bispectral IR camera, InAs/GaSb type-II superlattices (SLs) were selected as the IR photodetector material. InAs/GaSb type-II SLs consist of a periodic series of alternating InAs and GaSb layers with a thickness of merely a few atomic monolayers. The overlapping wave functions form a miniband for the electrons and enable optical transitions between the holes in GaSb and the electrons in InAs, which are used for the detection of IR radiation. The effective bandgap of this SL structure is lower than the bandgap of the constituting materials InAs and GaSb. Due to quantum confinement effects in thin layers (quantum films), carriers can only occupy well defined

eigenstates with discrete energy levels, defined by layer thickness and barrier height. Choosing adapted layer thickness values, typically between 5 – 15 atomic monolayers, the cut-off wavelength can be adjusted in the range of 3 – 30 µm. In Fig. 3, the bandgap energies and detector cut-off wavelengths are plotted versus the SL period for various combinations of InAs and GaSb monolayer thicknesses. There are suitable InAs/GaSb SL configurations for realising detection ranges all through the MWIR and LWIR spectral range. This so-called »bandgap engineering« on the atomic scale became feasible after the development of very precise molecular-beam epitaxial growth techniques, which allow the growth of different materials with a few atomic monolayer thickness and well defined interfaces. Note that this material system covers the whole MWIR and LWIR spectral range and can, therefore, be adapted for similar spectroscopic detector systems utilising specific spectral signatures of many other substances as well.

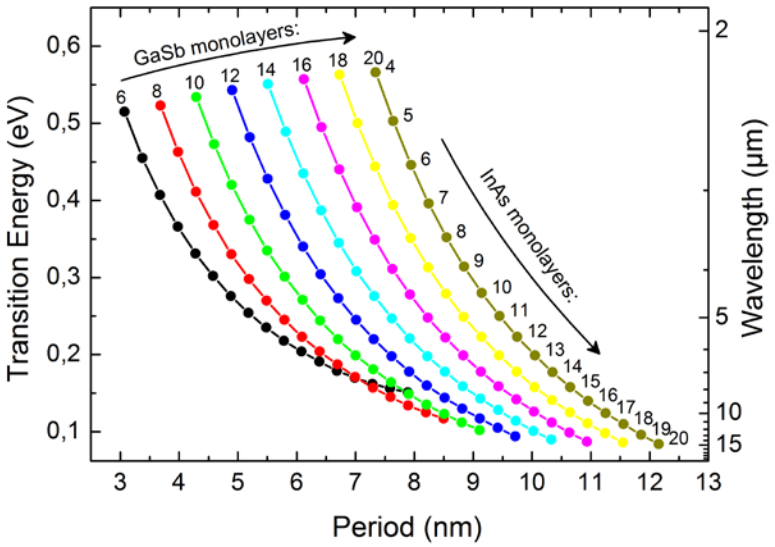

Fig. 3. *Transition energy and detection wavelength versus SL period for various numbers of InAs and GaSb monolayers within the InAs/GaSb type-II SL IR detector.*

The layer structure of the bispectral IR detector comprises two separate SL stacks for cut-off wavelengths around 4 µm (»blue channel«) and 5 µm (»red channel«), respectively [6]. In each stack, a p-i-n photodiode is realized by appropriate p- and n-doping. Both p-i-n diodes are placed back-to-back with a common p-type ground contact enabling the synchronous read-out of both diodes (Fig. 4a). Bispectral focal plane arrays are fabricated with 288 x 384 pixels at 40 µm pitch [7] on commercially available 3-inch GaSb wafers. Fig. 4b shows a scanning electron microscope (SEM) image of a part of a bispectral detector array. The individual camera pixels are separated by deep, narrow trenches. The two via holes per pixel, which give access to the common p-contact and »blue« n-contact, are visible as well as the three contact pads per pixel for the subsequent indium bump hybridisation with the read-out circuit.

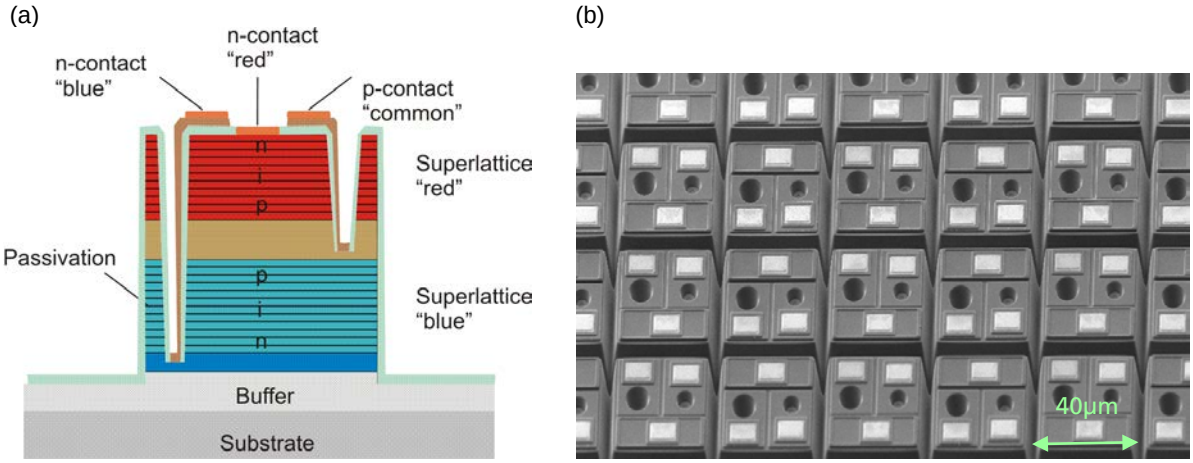

Fig. 4. *Schematic cross section of a bispectral detector pixel (a) and SEM image of a part of a processed bispectral detector array with 40 µm pixel pitch (b).*

4. Camera characterisation

In Fig. 5, the normalized photocurrent spectra of both, the red and the blue channel, are plotted versus wavelength. Furthermore, the spectral signature of the ($00^0$1) asymmetric stretching mode of CO_2 [1] is indicated as well. Since the detection range of the red channel spans the ($00^0$1) CO_2 mode in contrast to the blue channel, the red channel acts as a CO_2 sensitive channel and the blue channel as its reference channel. The cut-off wavelength of the red channel is not too close to 4.3 µm so that the ($00^0$1) CO_2 mode is covered by the red channel even in the case of a potential red-shift due to higher gas temperatures, which might occur in combustion processes.

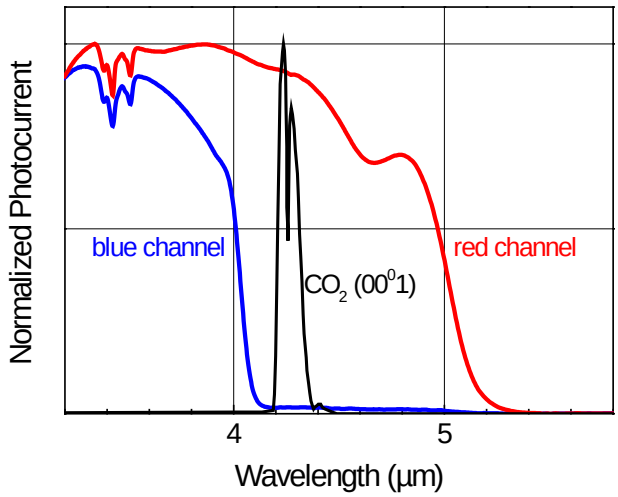

Fig. 5. *Normalized photocurrent spectra of the two channels of the bispectal IR camera and the absorption / emission spectrum of the asymmetric stretching mode of carbon dioxide.*

The thermal resolution is an important figure of merit for the performance of IR cameras. It is usually specified by the noise-equivalent temperature difference (NETD) representing the minimal temperature difference of a black body that can be distinguished by the detector, i.e. yields a signal-to-noise ratio equal to one. The NETD histograms for a 288 x 384 InAs/GaSb SL camera operated close to liquid-nitrogen temperature at half-well filling conditions (standard operating conditions) are presented in Fig. 6. Mean NETD values of 17.9 mK for the blue and 9.9 mK for the red channel have been determined.

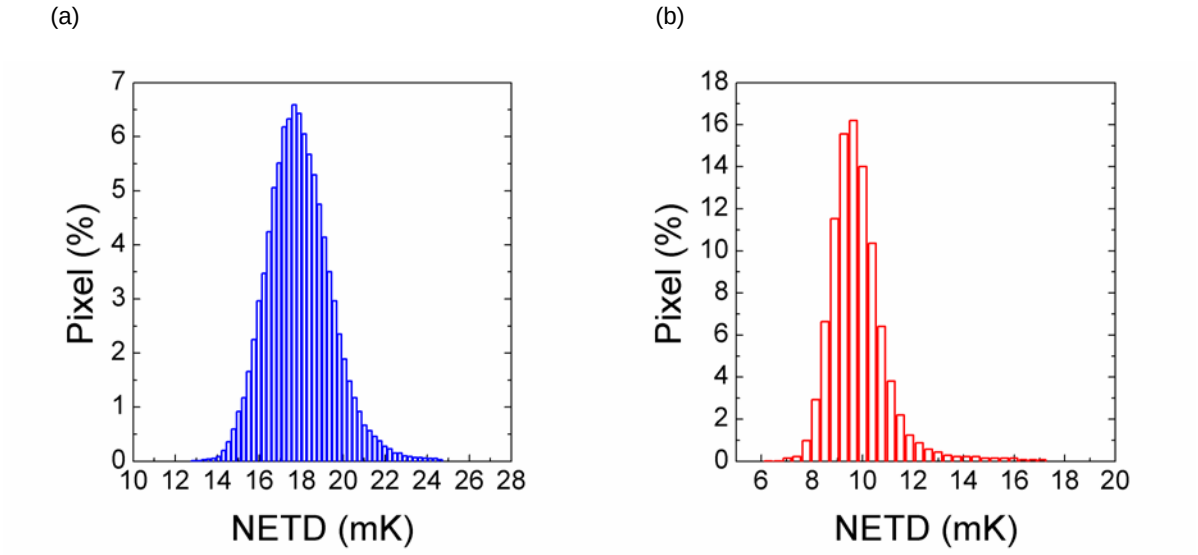

Fig. 6. *NETD histograms of the »blue« channel (a) and the »red« channel (b), respectively.*

http://dx.doi.org/10.21611/qirt.2012.233

5. CO_2 imaging

Fig. 7 shows a bispectral IR image of an industrial area, where the blue and red channels have been superimposed in blue and red color scales, respectively. IR radiation emitted by hot CO_2 at the top of smokestacks appears in red. In contrast, broadband thermal radiation from warmer surfaces cause a brighter shade of grey, while solar scattering in clouds in the sky or solar reflections from leaves or metallic surfaces even result in a pronounced blue signal. This way, the CO_2 emissions can be clearly distinguished from those other IR sources, which often cause false signatures in filter-based IR systems. The qualitative detection of CO_2 is so sensitive that even the CO_2 in the human breath can be visualised, see Fig. 8.

Fig. 7. *Bispectral IR image of an industrial area by a superposition of the two individual channels in a blue and a red color scale, respectively. The signatures of CO_2 emissions of smokestacks appear in red.*

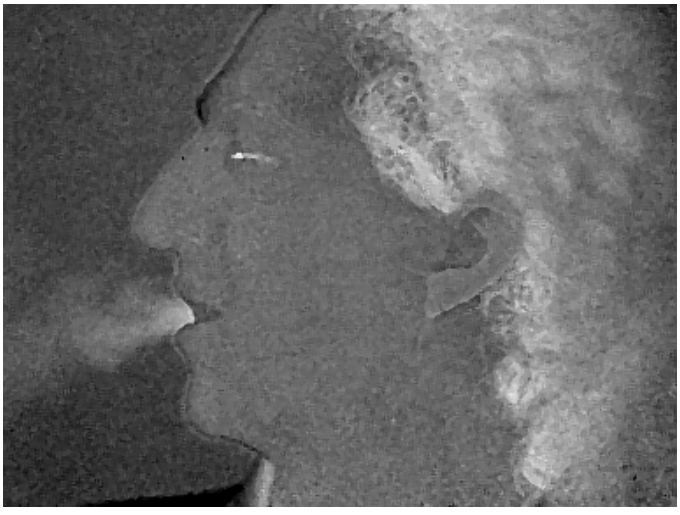

Fig. 8. *Bispectral IR image of an exhaling person by subtracting the »blue« channel from the »red« channel. The sensitivity is sufficient to visualise the CO_2 content in the exhalation air.*

6. Conclusion

We presented a bispectral IR camera comprising two detector channels manufactured from InAs/GaSb type-II superlattices. The detection bands of the two channels range from 3 – 4 µm and 4 – 5 µm, respectively. Thus, this camera is very sensitive to the asymmetric stretching mode of CO_2. Due to the stacked detector design, it can be used for remote imaging of CO_2 without the need for filter elements. The high thermal resolution with NETD values of 17.9 mK and 9.9 mK for the blue and red channel, respectively, even allows the detection of CO_2 in the human exhalation air.

Acknowledgements

The authors are grateful to S. Fibelkorn, M. Finck, H. Güllich, Th. Henkel, L. Kirste, and W. Luppold for detector processing, hybridisation, and characterisation. Project funding by the Federal Ministry of Defense is gratefully acknowledged.

REFERENCES

[1] M. Vollmer and K.-P. Möllmann, “Infrared Thermal Imaging”. Ch. 7, WILEY-VCH, Weinheim, 2010. ISBN 978-3-527-40717-0.
[2] D. L. Auble and T. P. Meyers, “An open path, fast response infrared absorption gas analyzer for H_2O and CO_2”, Boundary-Layer Meteorology, Vol. 59, pp. 243-256, 1992.
[3] G. P. Jellison and D. P. Miller, “Plume structure and dynamics for thermocouple and spectrometer measurements”, Proc. SPIE, Vol. 5425, pp. 232-243, 2004.
[4] G. M. Williams and A. Barter, “Dual-Band MWIR/LWIR Radiometer for Absolute Temperature Measurements”, Proc. SPIE Vol. 6205, 62050M, pp. 1-13, 2006.
[5] M. Abuhamad and U. Netzelmann, “Dual-band active thermography on infrared transparent materials”, Proc. 10th International Conference on Quantitative InfraRed Thermography, paper QIRT2010-001, Québec (Canada), 2010.
[6] R. Rehm, M. Walther, J. Schmitz, J. Fleißner, J. Ziegler, W. Cabanski, R. Breiter, “Dual-colour thermal imaging with InAs/GaSb superlattices in mid-wavelength infrared spectral range”. Electronics Letters Vol. 42, no. 10, pp. 577-578, 2006.
[7] F. Rutz, R. Rehm, J. Schmitz, J. Fleißner, M. Walther, R. Scheibner, J. Ziegler, “InAs/GaSb superlattice focal plane array infrared detectors: manufacturing aspects”. Proc. SPIE Vol. 7298, 729881R, pp. 1-10, 2009.